JPEDAV (2005) 26:494-502
DOI: 10-1361/154770305X66619
1547-7037/$19.00 ©ASM International

Analyses of Diffusion-Related Phenomena in Steel Process

Tooru Matsumiya

(Submitted July 19, 2005)

In steel production processes, there are various diffusion-related phenomena, and these are controlled to obtain the required steel quality. In the refining process, the slag-metal reaction that is controlled by the diffusion of various reactants and products in boundary layers in both the slag and metal side along the slag-metal interface is analyzed by a coupled reaction model. Solidification microsegregation is controlled by the solute diffusion in the liquid and solid phases, and various analytical microsegregation models have been proposed. The tertiary precipitation of nonmetallic inclusions is also affected by solute diffusion in the solid phase and is analyzed by a coupled precipitation model, the modified solidification segregation model. The formation of a carbon (C)-rich band structure along the centerline of steel plates and weld cracking are also prevented by regulating the diffusion of C by accelerated cooling and by encouraging hydrogen to diffuse out by preheating the weld part, respectively. A key element of intragranular ferrite precipitation for ferrite grain refinement is the formation of manganese (Mn)-depleted zone by slow Mn diffusion around a precipitate.

1. Introduction

Steel products of high quality are obtained by controlling, for example, chemical reactions, phase transformations, precipitation, and segregation in steel production and fabrication processes. Diffusion plays pivotal roles in these processes in many cases. Therefore, the proper control of the processes can be accomplished by the proper use of the effect of the diffusion. Diffusion-involved processes are discussed here: demanganization process of hot metal, segregation and precipitation during solidification processing, diffusion-controlled transformation process, welding, and coating process.

2. Refining Process

The refining of steel is conducted mainly by the use of the slag-metal reaction and injection metallurgy. In both cases, a chemical reaction occurs between liquid metal and refining agents that are frequently liquid oxides. The slag-metal refining process can be analyzed by a coupled reaction model developed by Robertson et al.[1] The reaction between the injected flux and the metal can be analyzed in the same manner. Figure 1 shows a schematic view of the model. In the model, thermodynamic equilibrium for each component oxide in the slag and for solutes in the metal is assumed at the slag-metal interface, and double diffusion layers are considered along the slag-metal interface. Chemical compositions in the bulk metal and the bulk slag outside the boundary layers are treated as uniform with respective concentrations. Concentrations in slag and metal at the slag-metal interface are calculated by the use of flux conservation equations of metal components and oxygen (O) across the double boundary layers and by thermodynamic equilibrium equations for component oxides with solute contents in the metal at the interface. In the case of carbon (C), a rate equation of carbon monoxide (CO) evolution is applied at the slag-metal interface instead of the local thermodynamic equilibrium $\underline{C} + \underline{O} = CO$, and a mass balance equation for

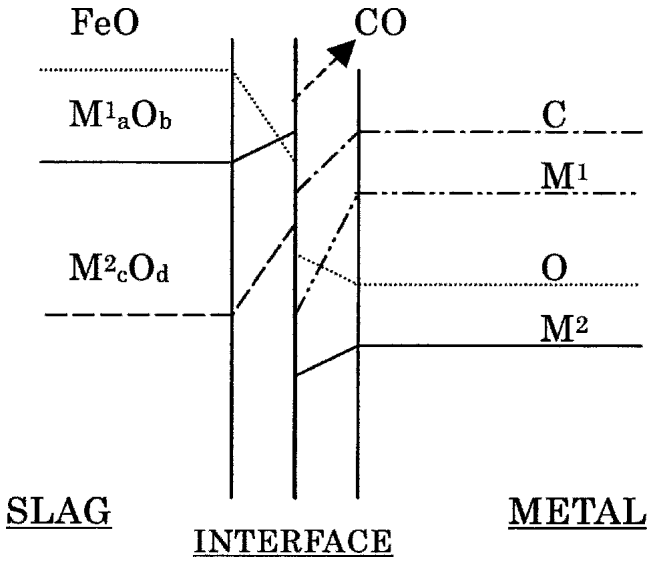

Fig. 1 Schematic diagram of the coupled reaction model

This article is a revised version of the paper printed in the *Proceedings of the First International Conference on Diffusion in Solids and Liquids—DSL-2005*, Aveiro, Portugal, July 6-8, 2005, Andreas Öchsner, José Grácio and Frédéric Barlat, eds., University of Aveiro, 2005.

Tooru Matsumiya, Technical Development Bureau, Nippon Steel Corporation 20-1 Shintomi, Futtsu-city, Chiba-prefecture, 283-9511 Japan. Contact e-mail: matumiya@re.nsc.co.jp.

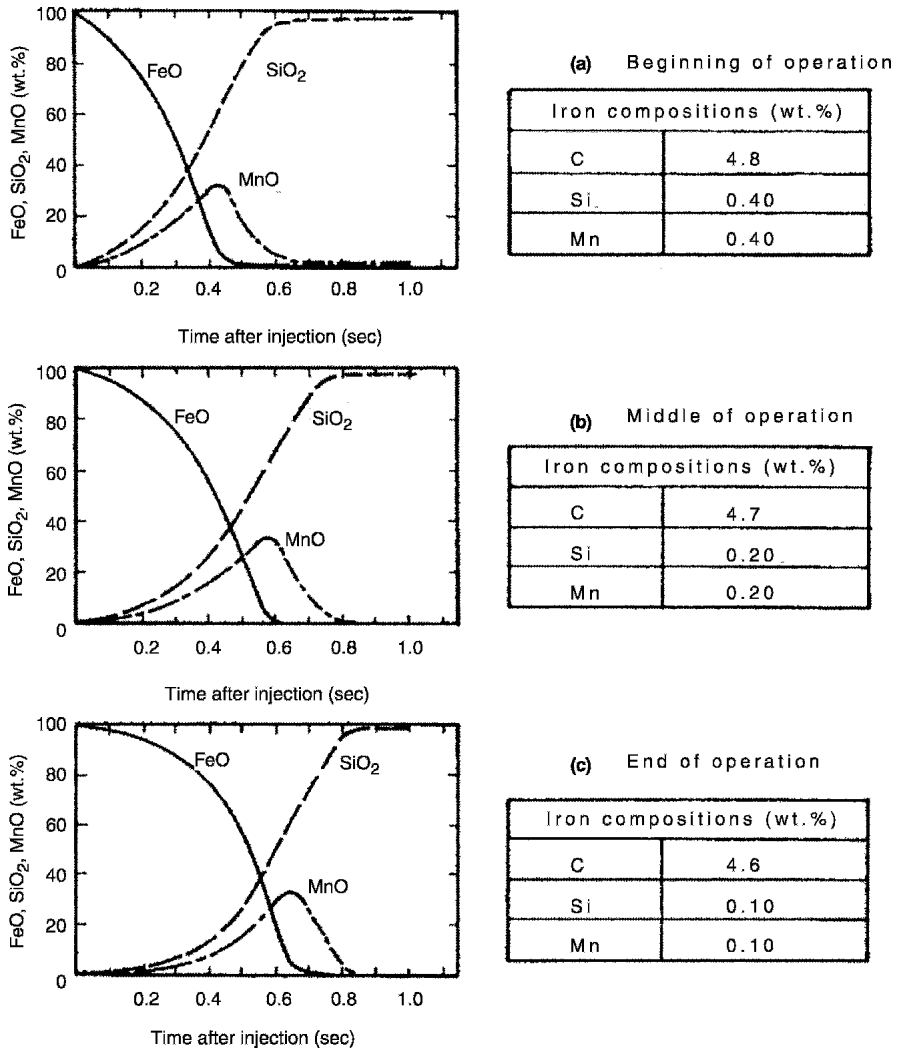

Fig. 2 Chemical composition changes in the refining powder after it is injected into hot metal in demanganization and desiliconization processes[2]

C between C flux from the metal and the CO evolution rate is considered.

Once the interfacial concentrations are determined, the flux of each metal component and O from the bulk metal to the bulk slag, or vice versa, as well as the CO evolution rate and decarburization rate, are obtained, and chemical composition changes in both the bulk slag and metal are calculated.

This model was applied to optimize the demanganization process of hot metal, where iron oxide (FeO) powder is injected in a hot metal through an immersed nozzle.[2] The chemical composition change of the injected powder is analyzed with the model. The results are shown in Fig. 2. The silica concentration increases, and the FeO concentration decreases monotonically, while the manganese oxide (MnO) concentration reaches its maximum and decreases as time elapses after the powder is injected. This is because the O potential in the powder is not enough to oxidize manganese (Mn) in hot metal after the MnO reaches its maximum and is reduced back to hot metal. Therefore, from the viewpoint of efficient demanganization, the injected powder is desired to float up to the top slag when the Mn concentration in the powder reaches the maximum. Because the time at the maximum Mn concentration becomes longer as the demanganization process proceeds due to less concentration in silicon and Mn in hot metal, the depth of nozzle immersion should be increased accordingly to realize efficient demanganization. According to this result, the demanganization process is conducted successfully.

3. Solidification Microsegregation

Depending on the degree of solute diffusion, several approximations can be made for the description of solidification microsegregation. Local thermodynamic equilibrium at the solid-liquid (S-L) interface and complete mixing of the solute in the liquid phase are always assumed in sections 3.1 through 3.4.

3.1 Equilibrium Solidification

When the solute is uniformly distributed over the respective solid and liquid phases, that is, when the whole system is in thermodynamic equilibrium, the solute concentration in the solid (C_S) is calculated by:

$$C_S = kC_0/\{1 - (1 - k)f_S\} \quad \text{(Eq 1)}$$

where C_0 is the average solute concentration, k is the equilibrium S-L partition coefficient, and f_S is the solid fraction.

3.2 The Scheil Equation

When the diffusion in the solid is completely neglected and complete mixing of solute in liquid is assumed, the equation of Scheil[3] applies:

$$C_S = kC_0(1 - f_S)^{k-1} \quad \text{(Eq 2)}$$

where C_S is the concentration in the solid at the S-L interface.

3.3 The Brody-Flemings Equation

When back-diffusion of solute into the solid phase from the S-L interface is considered, the equation of Brody and Flemings[4] is valid:

$$C_S = kC_0(1 - (1 - 2\alpha k)f_S)^{(k-1)/(1-2\alpha k)} \quad \text{(Eq 3)}$$

where α is the solidification parameter and is defined as $D_S t_S/L^2$, D_S is the diffusion coefficient in the solid phase, t_S is the local solidification time, and L is half of secondary dendrite arm spacing. In the derivation of Eq 3, the amount of back-diffusion is approximately calculated by $D_S(dC_S/Ldf_S)dt$, and the time increment dt is replaced by $2t_S f_S df_S$, assuming the parabolic growth law $f_S = (t/t_S)^{1/2}$.

3.4 The Clyne-Kurz Equation

Clyne and Kurz[5] corrected the overestimation of back-diffusion in the equation of Brody and Flemings[4] and proposed the following equation, replacing the solidification parameter α with Ω:

$$C_S = kC_0\{1 - (1 - 2\Omega k)f_S\}^{(k-1)/(1-2\Omega k)} \quad \text{(Eq 4)}$$

where Ω is defined by Eq 5:

$$\Omega = \alpha\{1 - \exp(-1/\alpha)\} - 1/2\exp(-1/2\alpha) \quad \text{(Eq 5)}$$

where Ω tends to 1/2 as α tends to infinity; that is, diffusion is complete and Eq 4 becomes Eq 1. Omega tends to α and then to 0, as α approaches 0. That is, Eq 4 tends to Eq 3 and then to Eq 2. Therefore, Eq 4 qualitatively covers all situations ranging from complete to zero mixing in the solid.

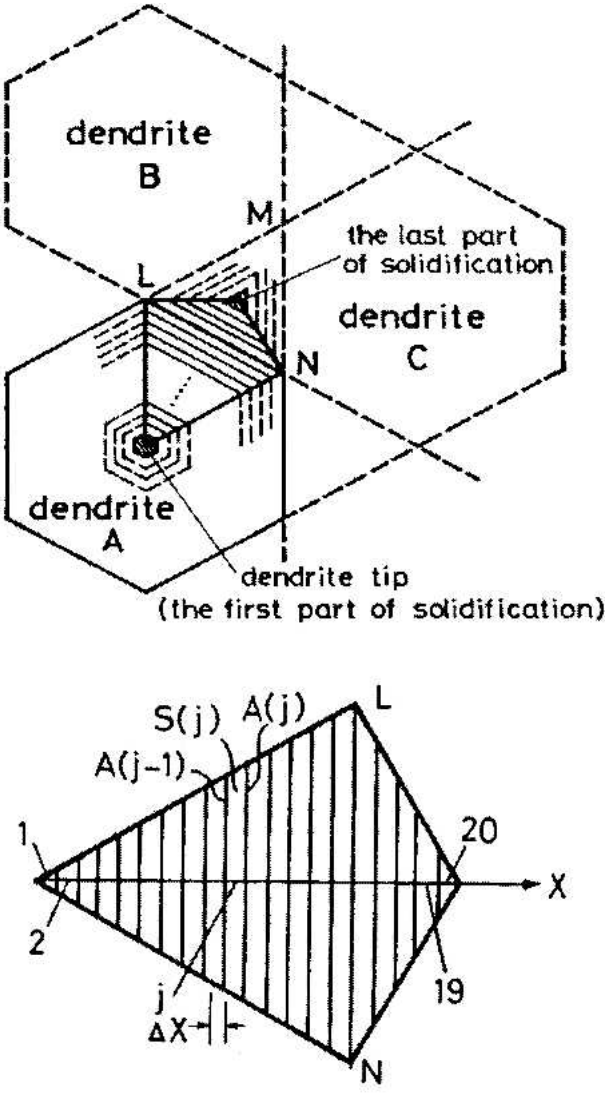

Fig. 3 (a) Model for a transverse cross section of dendrite and (b) the portion selected for analysis from the dendrite section[6]

3.5 Effective Partition Coefficient

When the complete mixing in the liquid cannot be assumed and the diffusion boundary layer along the S-L interface is considered, the effective S-L partition coefficient k_e is calculated by:

$$k_e = k/\{k + (1 - k)\exp(-R\delta/D_L)\} \quad \text{(Eq 6)}$$

where δ is the thickness of the diffusion boundary layer, R is the advancement velocity of the S-L interface, and D_L is the diffusion coefficient in liquid. As δ approaches 0 and infinity, k_e approaches k and 1, respectively.

3.6 Microsegregation Analysis by the Finite Difference Method

For quantitative preciseness, the finite difference method (FDM) was applied to analyze microsegregation. The trans-

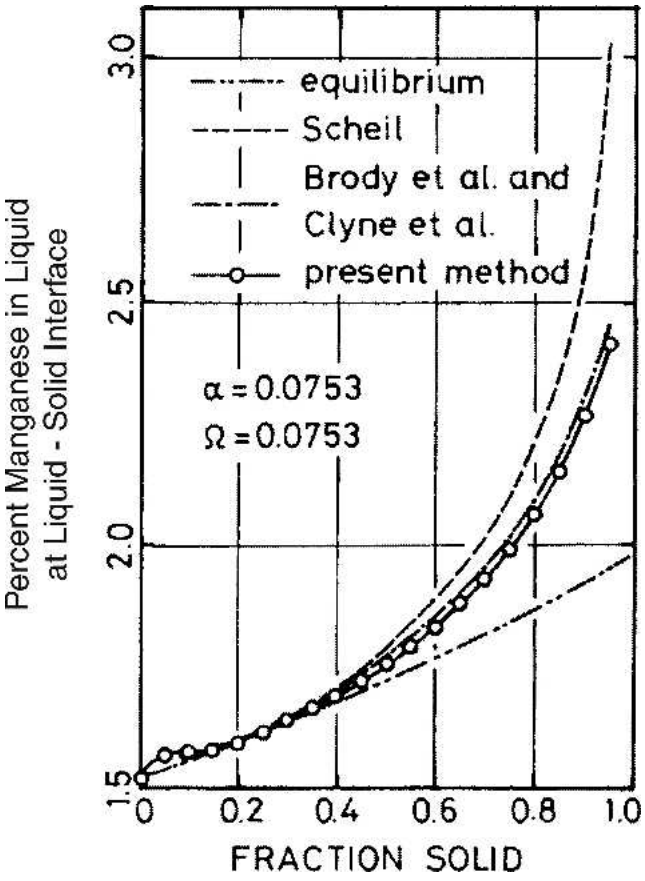

Fig. 4 Comparison of dendrite segregation calculated by various analytical methods[6]

verse cross section of a dendrite is approximated as a hexagonal shape, and a double-triangle section, as shown in Fig. 3, is chosen for analysis considering the symmetry of diffusion and neglecting the diffusion along the axial direction of the dendrite. The double-triangle section is divided into finite segments, and solute diffusion in the radial direction is calculated by the use of the FDM. The solute content in each segment is updated, and the thermodynamic equilibrium calculation is conducted in each time step in the segment where solid and liquid coexist using the updated average content. The calculated fractions of liquid and solid give the interface location. Figure 4 shows the simulated results of Mn concentration in comparison with microsegregation values calculated by the other model equations mentioned above.[6]

By the use of a similar method of analysis with consideration of solid-to-solid transformation (i.e., δ-to-γ transformation as well as liquid-to-solid transformation[7,8]), the solidification structure of the welding of stainless steels was analyzed, and the residual δ fraction, which affects the weld cracking, was estimated to be in agreement with observations, as shown in Fig. 5.[8]

Regarding the diffusion-controlled transformation and precipitation analysis, DICTRA[9] is one of the integrated analytical software that is based on the combinations of

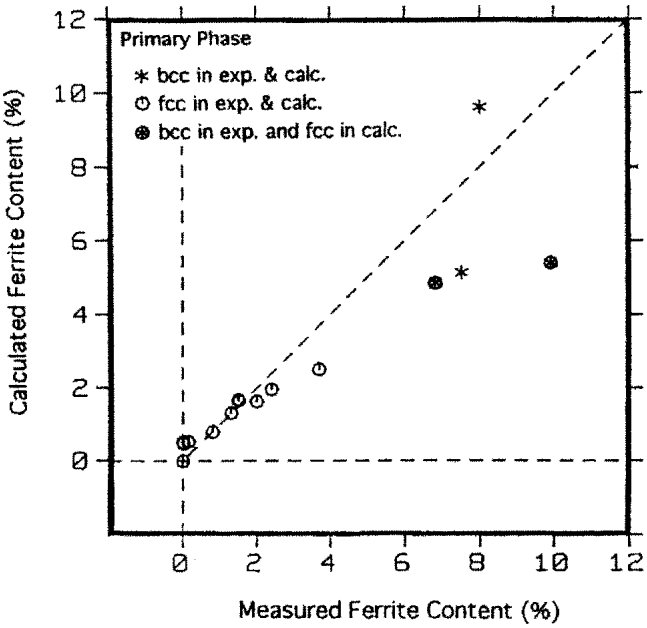

Fig. 5 Comparison of retained δ ferrite content between calculation and measurement[7]

multicomponent diffusion analysis by FDM and local thermodynamic equilibrium analysis at the interfaces.

4. Precipitation of Nonmetallic Inclusions

The coupled precipitation model[10] was developed to analyze the chemical composition change of nonmetallic inclusions during the solidification of steels. The basic equations are as follows:

$$(1-k)C_L^i df_S = \{1-(1-2\Omega^i k^i)f_S\}dC_L + \Sigma R_{ij}dP_j \qquad \text{(Eq 7)}$$

where super suffix i indicates the kind of solute, R_{ij} represents moles of element i in the precipitate j, and P_j is the concentration of precipitate j. If the last term in Eq 7 is omitted, Eq 7 becomes the solute conservation equation, the differential form of Eq 4.

Equation 7 is solved with the mass action equation of precipitation:

$$\pi\, a_i^{Rij}\, a_j = K_j \qquad \text{(Eq 8)}$$

where a_i is the activity of element i, a_j is the activity of precipitate j, and K_j is the equilibrium constant of precipitate j. That is, in the coupled precipitation model solidification microsegregation is analyzed with consideration of the back-diffusion of solutes into solid and local thermodynamic equilibrium assumed in the residual liquid, including the precipitation of nonmetallic inclusions (Fig. 6).

The model was applied to the analysis of sulfide shape control in steel for line pipe. When Mn sulfide (MnS) precipitates at the spot-like segregation along the centerline in a slab of this steel, it is elongated during plate rolling, and

the formation of a film-like MnS occurs in the thickness center of the line pipe produced, which acts as the initiation site of hydrogen (H)-induced cracking (HIC). To prevent MnS precipitation, calcium (Ca) is added to capture sulfur (S) in the form of Ca sulfide (CaS).

Figures 7 and 8 compare the calculated results of the change in chemical composition of nonmetallic inclusions during the solidification of spot-like segregation with diameters of 100 and 1000 μm. Spot-like segregation is formed by the localization of solute-enriched liquid, which is squeezed out from the interdendrite region by slab bulging and solidification shrinkage along the centerline in slabs. The average concentrations at the spot-like segregation are approximately the same as the solute concentrations in the residual liquid between the dendrites at a solid fraction of 0.9. Table 1 lists the average concentrations of line pipe steel and the concentrations at the spot-like segregation.

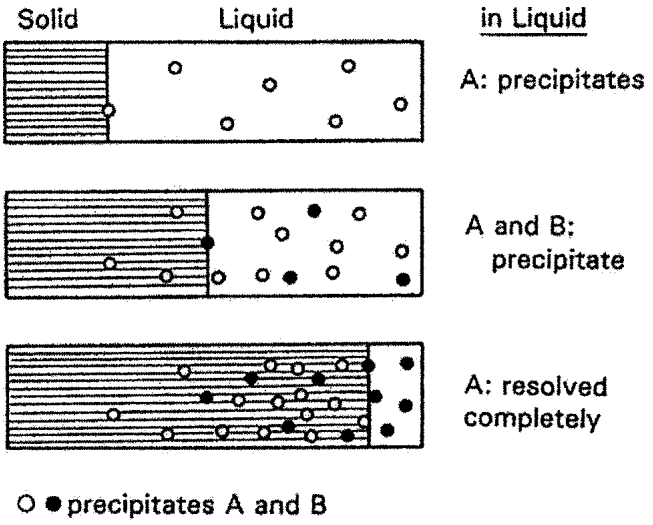

Fig. 6 Schematic diagram of the coupled precipitation model[10]

At the beginning of the solidification of a spot-like segregation with a diameter of 100 μm, O is mostly trapped in the form of Ca aluminate (C-A), and the rest of the Ca is used up for capturing S as CaS. The dissolved O content is <1 ppm, and dissolved Ca is around 1/100 ppm. The dissolved aluminum (Al) content is about 200 ppm, and the dissolved S content is about 70 ppm. As solidification proceeds, segregating S decomposes Ca oxide (CaO) in C-A forming CaS, and decomposed O is trapped by dissolved Al forming alumina (Al_2O_3). As the result, the Al_2O_3 content in C-A and the CaS concentration increase as the solid fraction increases. Because CaO in C-A does not decompose completely even at the end of solidification, segregated S is captured as CaS throughout solidification, and the precipitation of MnS is prevented in this case.

In the case of the solidification of a spot-like segregation with a diameter of 1000 μm, the general behavior of the chemical composition change of nonmetallic inclusions is

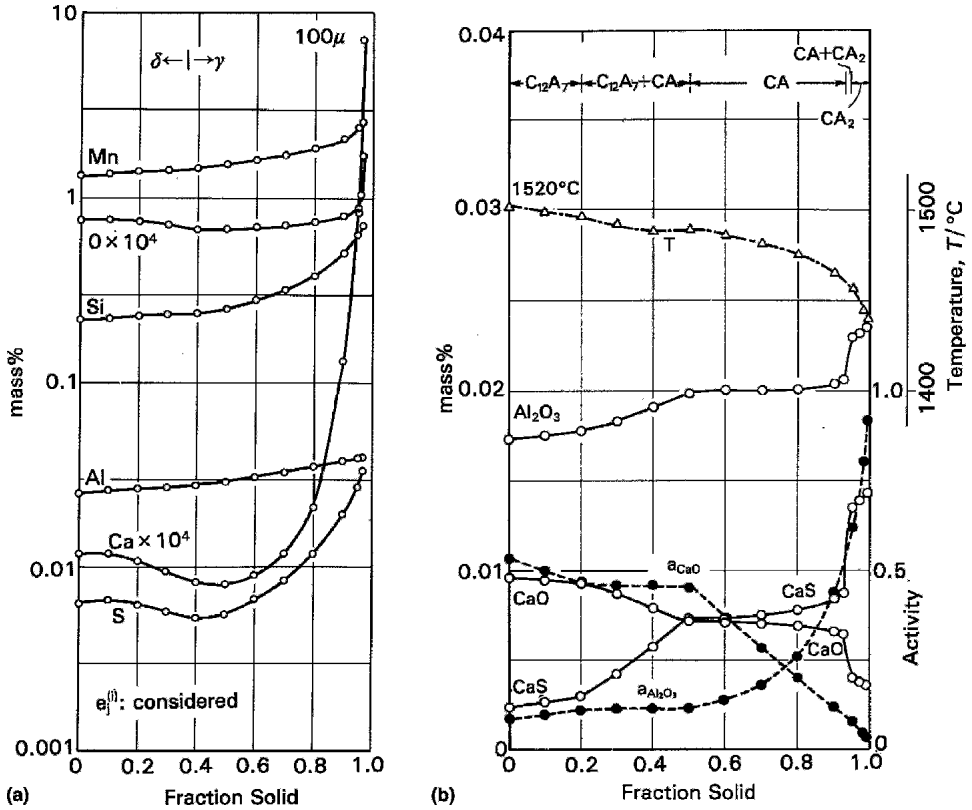

Fig. 7 (a) Changes in the amount of dissolved solutes and (b) nonmetallic inclusions in the residual liquid during solidification of a spot-like segregation with a diameter of 100 μm (calculated values)[10]

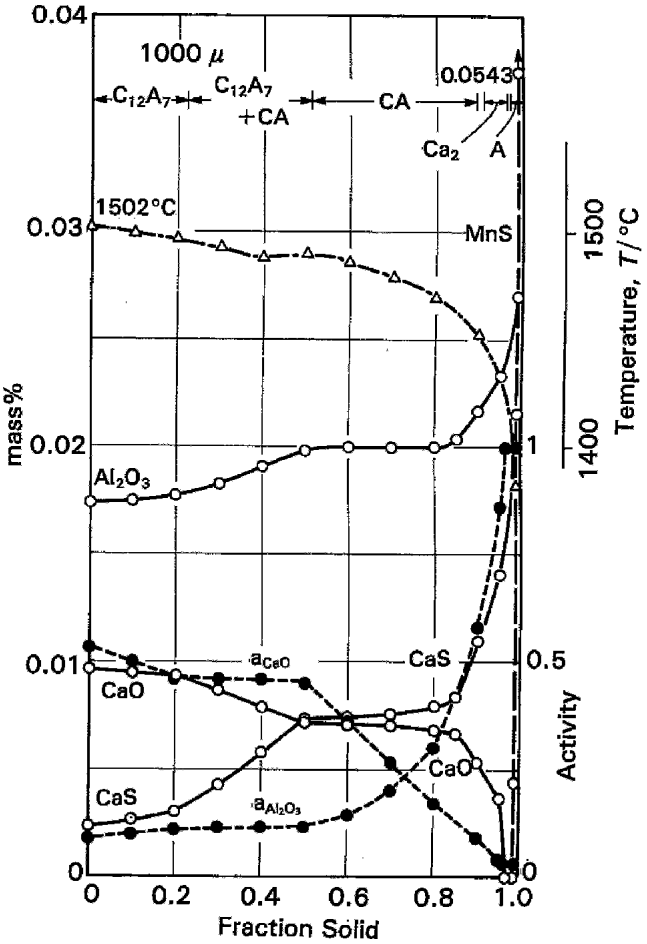

Fig. 8 The calculated change in amounts of nonmetallic inclusions in the residual liquid during the solidification of a spot-like segregation with a diameter of 1000 μm[10]

Table 1 Chemical composition of anti-hydrogen-induced cracking steel on average and in the residual liquid of growing dendrite at solid fraction of 0.9 (calculated value)[10]

	C	Si	Mn	P	S	Al	Ca	O
Average	0.081	0.16	1.02	0.0050	0.0012	0.0290	0.0033	0.0025
C_t^{90}	0.317	0.218	1.32	0.0203	0.0090	0.0447	0.0270	0.0270

Note: Values given as %

quite the same as that in the case of a spot-like segregation with a diameter of 100 μm. However, CaO decomposes completely at the very end of solidification. After that, there is no source of Ca for capturing segregating S, and the result is that MnS precipitates at the end. Sulfide shape control is not successful in this case. Because the back-diffusion of S is smaller, S enrichment in the residual liquid is higher, consuming CaO in C-A faster in a larger spot-like segregation than in smaller one. To prevent the precipitation of MnS, the size of the spot-like segregation should be regulated in addition to the proper amount of addition of Ca, which can be done by the minimization of slab bulging and the soft reduction of slab thickness near the crater end to compensate for thermal and solidification shrinkage.

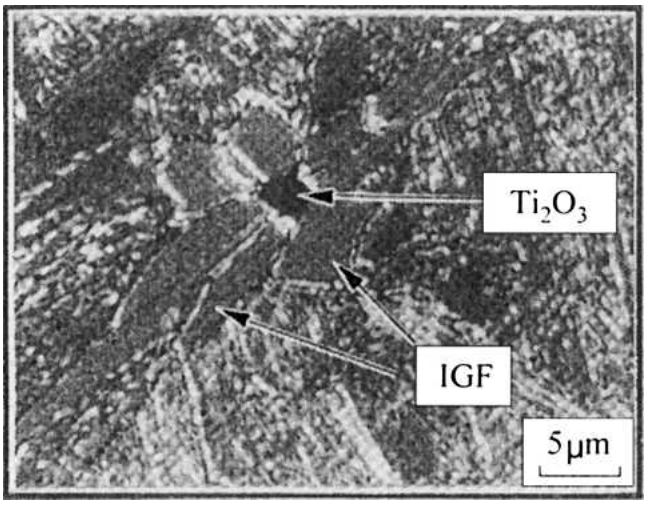

Fig. 9 Intragranular ferrite precipitation at Ti_2O_3[12]

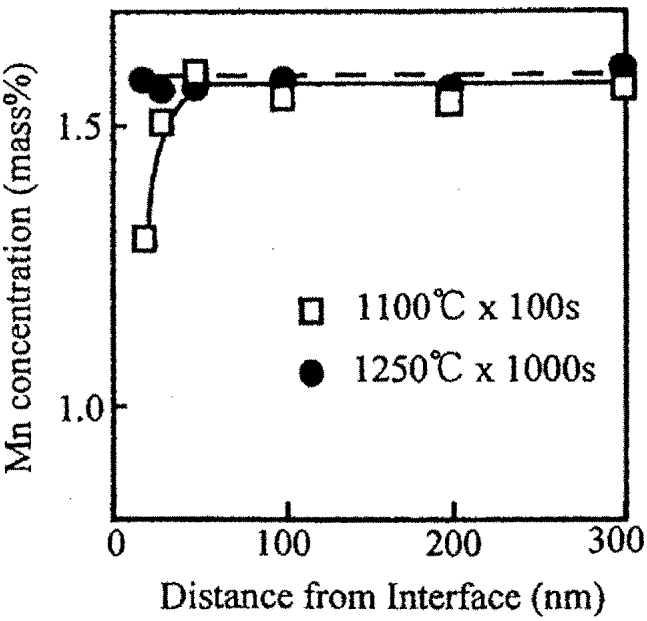

Fig. 10 The Mn concentration near the MnS-αFe interface[13]

5. Transformations in the Solid Phase

5.1 Band Structure Formation

Because austenite (γ)-to-ferrite (α) transformation takes place from the outside of a steel plate during thermomechanical processing, C ejected at the γ-α transformation front diffuses into residual γ phase, and the C content in the

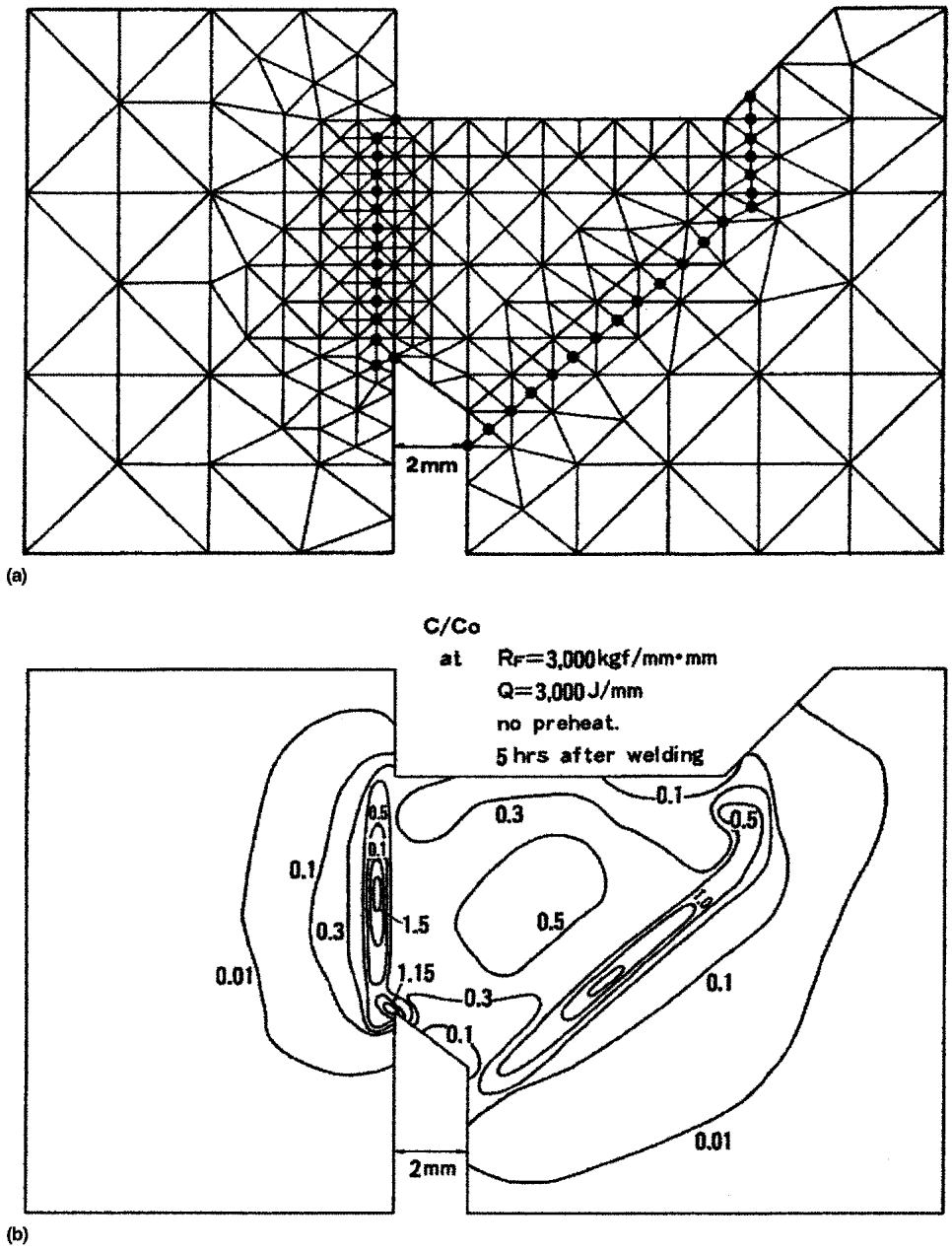

Fig. 11 (a) Element system for H diffusion in a weld by FDM and (b) calculated H distribution[14]

thickness center of the plate, the last part of the γ-to-α transformation, becomes extremely high and forms perlite bands when the cooling rate of the plate is low during the γ-to-α transformation. By the use of accelerated cooling during this period, the inward diffusion of C is regulated, and by stopping the accelerated cooling above the martensite transformation temperature the formation of perlite bands and martensite along the thickness center of produced plates is prevented, which is favorable for the prevention of crack propagation and initiation.[11]

5.2 Intragranular Ferrite Precipitation

In the γ-to-α transformation temperature range, ferrite precipitates in titanium oxide inside a γ grain (Fig. 9),[12] which is called intragranular ferrite (IGF) precipitation, and contributes to ferrite grain refinement and the production of steel plates with high degrees of strength and toughness. The best conditions for IGF precipitation are a heterogeneous nucleation site and a C or Mn-depleted zone, which is favorable for ferrite stability.

Shigesato et al.[13] showed the existence of an Mn-depleted zone around MnS in a properly heat-treated steel that acted as an IGF precipitation site (Fig. 10).

6. Welding

Because the welding pool temperature reaches 10,000 °C, H from the ambient atmosphere and rust dissolve

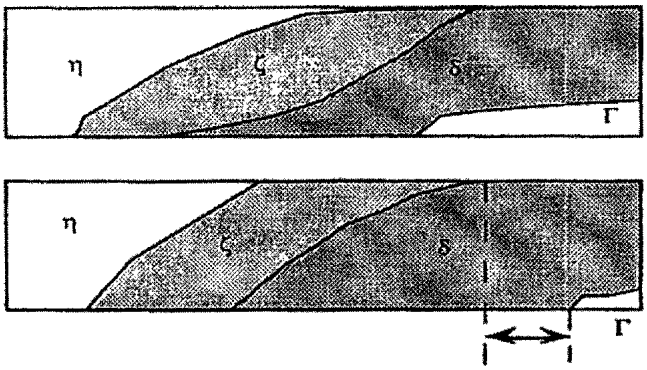

Fig. 12 Schematic view of interdiffusion and phase transformation in a Zn coating during heat treatment

in the pool. The apparent activity coefficient of H after welding varies from location to location depending on the stress-and-strain field (i.e., dislocation distribution) formed during solidification and cooling. Figure 11 shows the calculated H distribution near the weld part taking these factors into consideration.[14] The calculated results indicate H enrichment in the heat-affected zone (HAZ), where high microvoid density is assigned. For this reason, welding cracks propagate along the HAZ. However, when preheating is conducted in advance of welding, the cooling rate of the weld part is reduced, concomitantly, the out-diffusion of H is encouraged during the cooling, H concentration in the HAZ is lowered, and weld cracking is prevented.

7. Galvanic Alloy Coating

Because the zinc (Zn) η phase has a tendency to stick to the metal mold during the sheet pressing, an Fe-Zn intermetallic compound phase, δ, which has less sticking tendency and is rather lubricative against the press mould, is preferred for coating the surface of steel sheets. This phase can be produced by Fe-Zn interdiffusion during the heat treatment after Zn coating of the steel sheets. Because another Fe-Zn intermetallic compound phase, Γ, that is richer in Fe than the δ phase is brittle and causes powdering during the forming of coated sheets, Fe-Zn interdiffusion should be regulated not to form this phase while forming the δ phase. Although it is thought that the interdiffusion and formation of various intermetallic phases should be analyzed simply, as shown in Fig. 12, the fact that the interface energy between various phases affects the nucleation of a new phase, that the interface energy and growth rate of various phases have crystal orientation dependency, and that grain boundary diffusion affects the reaction make the analysis much more complicated.

8. Conclusions

Analyses of various diffusion-related phenomena in steel production process were discussed:

- The refining process was analyzed by the coupled reaction model, in which the diffusion of solutes in the metal diffusion boundary layer and the diffusion of component oxides and sulfides in the slag diffusion boundary layer along the slag-metal interface are calculated, and the local thermodynamic equilibrium of each component oxide and sulfide in the slag with solute concentration in the metal and a kinetic equation for the evolution rate of CO was applied at the slag-metal interface. As an example, the demanganization process of hot metal by FeO was mentioned.
- Solidification microsegregation was analyzed by modeling the diffusion of solutes, especially in the solid phase or numerically by FDM. The Mn microsegregation calculated by FDM and various analytical equations for microsegregation were compared, and a method for the estimation of the residual ferrite content in the weld pool in the Fe-Cr-Ni alloy by FDM was shown.
- The change in chemical composition of nonmetallic inclusions during the solidification of steel was analyzed by the coupled precipitation model, in which the solidification microsegregation of solutes is analyzed with consideration of their back-diffusion and the local thermodynamic equilibrium is assumed in the residual liquid including the precipitation of nonmetallic inclusions in the liquid. The model was applied to sulfide shape control in anti-HIC steel for line pipes, and it was elucidated that MnS precipitation cannot be prevented even with the proper addition of Ca when the size of a spot-like segregation exceeds a threshold due to the lack of effectiveness of the back-diffusion of S.
- The formation of perlite bands as well as micromartensite is eliminated in steel plate production by deceleration of C diffusion by accelerated cooling during austenite-ferrite transformation that is stopped at a temperature above that of martensitic transformation.
- Intragranular ferrite nucleation at Ti_2O_3 in γ grain is encouraged by the formation of an Mn-depleted zone around growing MnS due to slow diffusion of Mn in the matrix, which was analyzed by calculation and transmission electron microscopy observation.
- Hydrogen diffusion and distribution were analyzed by FDM in the welding, which comes into welding from the moisture of the atmosphere, and it was elucidated that preheating of the weld parts to 200 °C made H to diffuse out and eliminated the formation of the H-enriched region in the heat-affected zone, which resulted in the prevention of weld cracking.
- In the Zn alloy coating, the formation of a δ phase with limited formation of a Γ phase, which is brittle and causes powdering during the pressing of coated sheets, by the control of Fe-Zn interdiffusion is the key issue.

References

1. D.G.C. Robertson, B. Deo, and S. Oguchi, Muticomponent Mixed-Transport-Control Theory for Kinetics of Coupled Slag/Metal and Slag/Metal/Gas Reactions: Application to

Desulphurization of Molten Iron, *Ironmaking Steelmaking,* Vol 11, 1984, p 41-55
2. T. Kitamura, K. Shibata, I. Sawada, and S. Kitamura, Optimization of Refining Process by Computer Simulation, *Bull. Jpn. Inst. Metals,* Vol 28, 1989, p 310-312 (in Japanese)
3. E. Scheil, Bemerkugen zur Schichtkristallbildung *Z. Metallkd.,* Vol 34, 1942, p 70-72 (in German)
4. H.D. Brody and M.C. Flemings, Solute Redistribution in Dendritic Solidification, *Trans. Metall. Soc. AIME,* Vol 236, 1966, p 615-634
5. T.W. Clyne, and W. Kurz, Solute Redistribution During Solidification with Rapid Solid State Diffusion, *Metall. Trans. A,* Vol 12, 1981, p 965-971
6. T. Matsumiya, H. Kajioka, S. Mizoguchi, Y. Ueshima, and H. Esaka, Mathematical Analysis of Segregation in Continuously-Cast Slabs, *Trans. ISIJ,* Vol 24, 1984, p 873-882
7. Y. Ueshima, S. Mizoguchi, T. Matsumiya, and H. Kajioka, Analysis of Solute Distribution in Dendrites of Carbon Steel with δ/γ Transformation during Solidification, *Metall. Trans. B,* Vol 17, 1986, p 845-859
8. T. Koseki, T. Matsumiya, W. Yamada, and T. Ogawa, Numerical Modeling of Solidification and Subsequent Transformation of Fe-Cr-Ni Alloys, *Metall. Mater. Trans. A,* Vol 25, 1994, p 1309-1321
9. J. Agren, Numerical Treatment of Diffusional Reaction in Multicomponent Alloys, *J. Phys. Chem. Solids,* Vol 43, 1982, p 385-391
10. T. Matsumiya, Mathematical Analyses of Segregations and Chemical Compositional Changes of Nonmetallic Inclusions during Solidification of Steels, *Trans. JIM,* Vol 33, 1992, p 783-794
11. H. Tamehiro, R. Habu, N. Yamada, H. Matsuda, and M. Nagumo, Properties of Large Diameter Line Pipe Steel Produced by Accelerated Cooling After Controlled Rolling, *Proceedings of the International Symposium on Accelerated Cooling of Steel,* P.D. Southwick, Ed., AIME, 1986, p 401-413
12. J. Takamura and S. Mizoguchi, Role of Oxides in Steels Performance: Metallurgy of Oxides in Steels, *Proceedings of the 6th International Iron and Steel Congress,* Vol 1, The Iron and Steel Institute of Japan, 1990, p 591-597
13. G. Shigesato, M. Sugiyama, S. Aihara, R. Uemori, and H. Furutani, Influence of Mn-Depleted Zone on Intragranular Ferrite Formation in HAZ of Low Alloy Steel (2), *CAMP-ISIJ,* Vol 12, 1999, p 1294 (in Japanese)
14. N. Yurioka, S. Ohshita, H. Nakamura, and K. Asano, An Analysis of Effects of Micro-Structure, Strain and Stress on the Hydrogen Accumulation in the Weld Heat-Affected Zone, *IIW Doc.,* 1980, 1X-1161-80